Antigen cross-presentation in young tumor-bearing hosts promotes CD8$^+$ T cell terminal differentiation

Ardiana Moustaki[1], Jeremy Chase Crawford[1], Shanta Alli[1], Yiping Fan[2], Shannon Boi[1], Anthony E Zamora[1], Natalie M N McDonald[1,5], Gang Wu[2], Joy Nakitandwe[3], Scott Newman[4], Scott Foy[4], Antonina Silkov[4], Paul G Thomas[1], Alberto Pappo[6], Michael A Dyer[7,8], Elizabeth Stewart[6,7], Sara Federico[6], Ben Youngblood[1*]

[1] Department of Immunology, St. Jude Children's Research Hospital, Memphis, TN 38105, USA
[2] Center for Applied Bioinformatics, St. Jude Children's Research Hospital, Memphis, TN 38105, USA
[3] Department of Pathology, St. Jude Children's Research Hospital, Memphis, TN 38105, USA
[4] Department of Computational Biology, St. Jude Children's Research Hospital, Memphis, TN 38105, USA
[5] University of Tennessee Health and Science Center (UTHSC) - Memphis, TN 38163
[6] Department of Oncology, St. Jude Children's Research Hospital, Memphis, TN 38105, USA
[7] Department of Developmental Neurobiology, St. Jude Children's Research Hospital, Memphis, TN 38105, USA
[8] Department of Ophthalmology, University of Tennessee Health Science Center, Memphis, TN 38105, USA

Keywords: T cell exhaustion, tumor microenvironment, age, antigen cross-presentation, pediatric tumors.

**Correspondence*: Benjamin.Youngblood@stjude.org

Supplementary figures

28 **Figure S1**

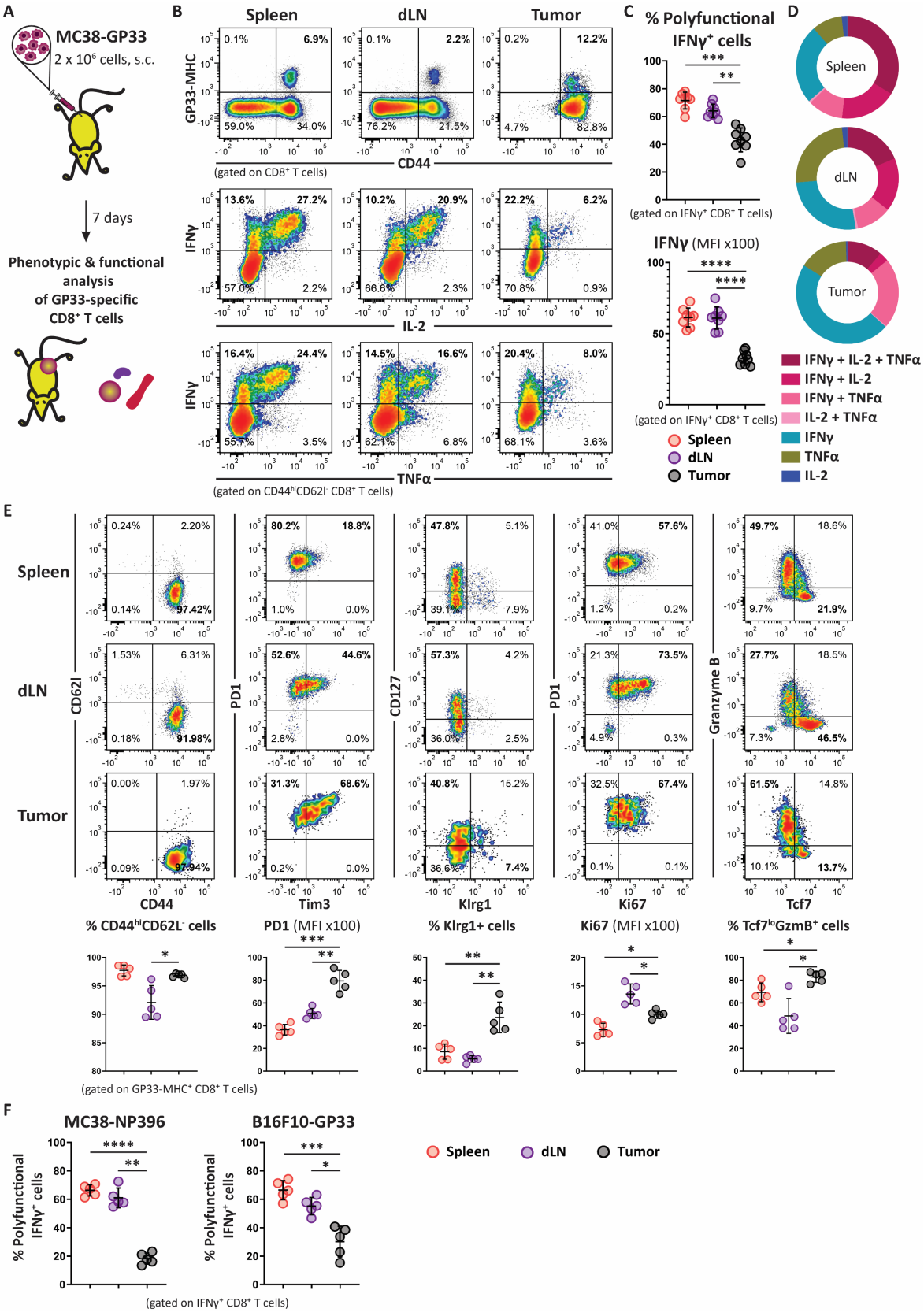

29

Figure S1 Antigen specific CD8$^+$ T cells that infiltrate the tumors are functionally impaired compared to corresponding cells in peripheral lymphoid organs.

(**A**) Schematic experimental design for panels (A-E): One to two million MC38-GP33 tumor cells were transplanted subcutaneously to immunocompetent, syngeneic (H-2b) hosts. One week later endogenous GP33-specific CD8$^+$ T cells isolated from peripheral lymphoid tissues or tumors were analyzed.

(**B**) Representative flow cytometry density plots showing the frequency of endogenous GP33-specific CD8$^+$ T cells (upper row) from the indicated tissues of TB mice and their potential to produce cytokines upon *ex vivo* stimulation with cognate peptide (2 bottom rows).

(**C**) Statistical analysis (n=8) of the cytokine profile shown in (B). Percent polyfunctionality is calculated as the percentage of IFNγ producing cells that also co-produce TNFα or IL-2. Mean $\pm$SD; unpaired one-way Anova with Tukey correction.

(**D**) Functional composition of CD8$^+$ T cells is summarized in the pie charts, which are color-coded according to the polyfunctionality of CD8$^+$ T cells (n=8).

(**E**) Expression profile of differentiation (CD44, CD62L, Klrg1, CD127, TCF7), activation (PD1, Tim3), proliferation (Ki67), and effector molecule (Granzyme B) markers, on GP33-specific CD8$^+$ T cells from the indicated organs, 7 days post MC38-GP33 tumor cell transplantation on C57Bl6 mice. Summarized data for each marker are shown on the right of the corresponding flow plots. Mean $\pm$SD; unpaired one-way Anova with Tukey correction.

(**F**) One million MC38-NP396 or B16F10-GP33 tumor cells were transplanted subcutaneously to immunocompetent, syngeneic (H-2b) hosts (n=5). One week later endogenous NP396-specific or GP33-specific CD8$^+$ T cells isolated from peripheral lymphoid tissues or tumors were analyzed. Summarized data showing the frequency of polyfunctional IFNγ^+ CD8$^+$ T cells upon *ex vivo* stimulation withNP396 or GP33 peptide respectively. Mean $\pm$SD; unpaired one-way Anova with Tukey correction.

A *p*-value of <0.05 is regarded as statistically significant, and different levels of significance are represented with asterisks: *P ≤ 0.05, **P ≤ 0.01, ***P ≤ 0.001, and ****P ≤ 0.0001.

56 **Figure S2**

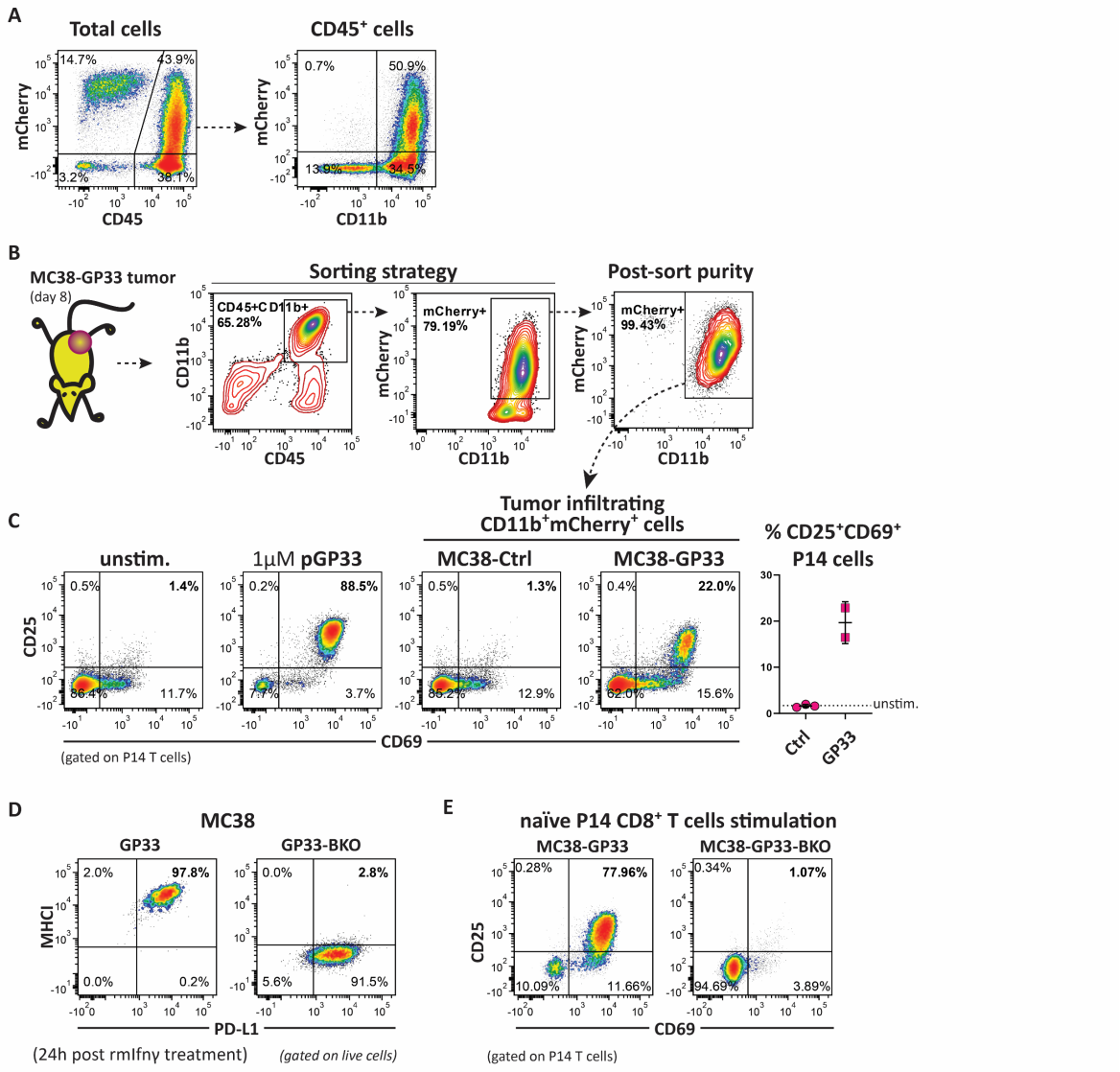

57

Figure S2 Tumor infiltrating myeloid cells can uptake and cross-present tumor antigens.

(**A**) Representative flow cytometry density plot showing detection of mCherry fluorescence in the tumor infiltrating leukocytes ($CD45^+$ cell fraction).

(**B**) Flow cytometry-based cell sorting strategy of tumor infiltrating $CD45^+CD11b^+mCherry^+$ cells from MC38-GP33 or MC38-Ctrl tumors established for 8 days in B57Bl6 mice.

(**C**) *In vitro* stimulation assay showing expression of early activation markers (CD25 and CD69) by naïve P14 $CD8^+$ T cells (responders) upon 4-hour coculture with $CD11b^+mCherry^+$ cells (stimulators) isolated from MC38-Ctrl (n=3) or MC38-GP33 (n=2) tumors. Unstimulated (negative control) and peptide-stimulated (positive control) P14 $CD8^+$ T cells are shown for reference. The experiment was performed once.

(**D**) CRISPR-mediated ablation of B2m gene blocks expression of MHC class I molecules on the surface of MC38-GP33 tumor cells. Cells were treated with 20 ng/mL of rmIfng for 24h.

(**E**) *In vitro* stimulation assay showing expression of early activation markers (CD25 and CD69) by naïve P14 $CD8^+$ T cells upon 4-hour coculture with MC38-GP33 cell sufficient or deficient in MHCI.

A *p*-value of <0.05 is regarded as statistically significant, and different levels of significance are represented with asterisks: $*P \leq 0.05$, $**P \leq 0.01$, $***P \leq 0.001$, and $****P \leq 0.0001$.

Figure S3

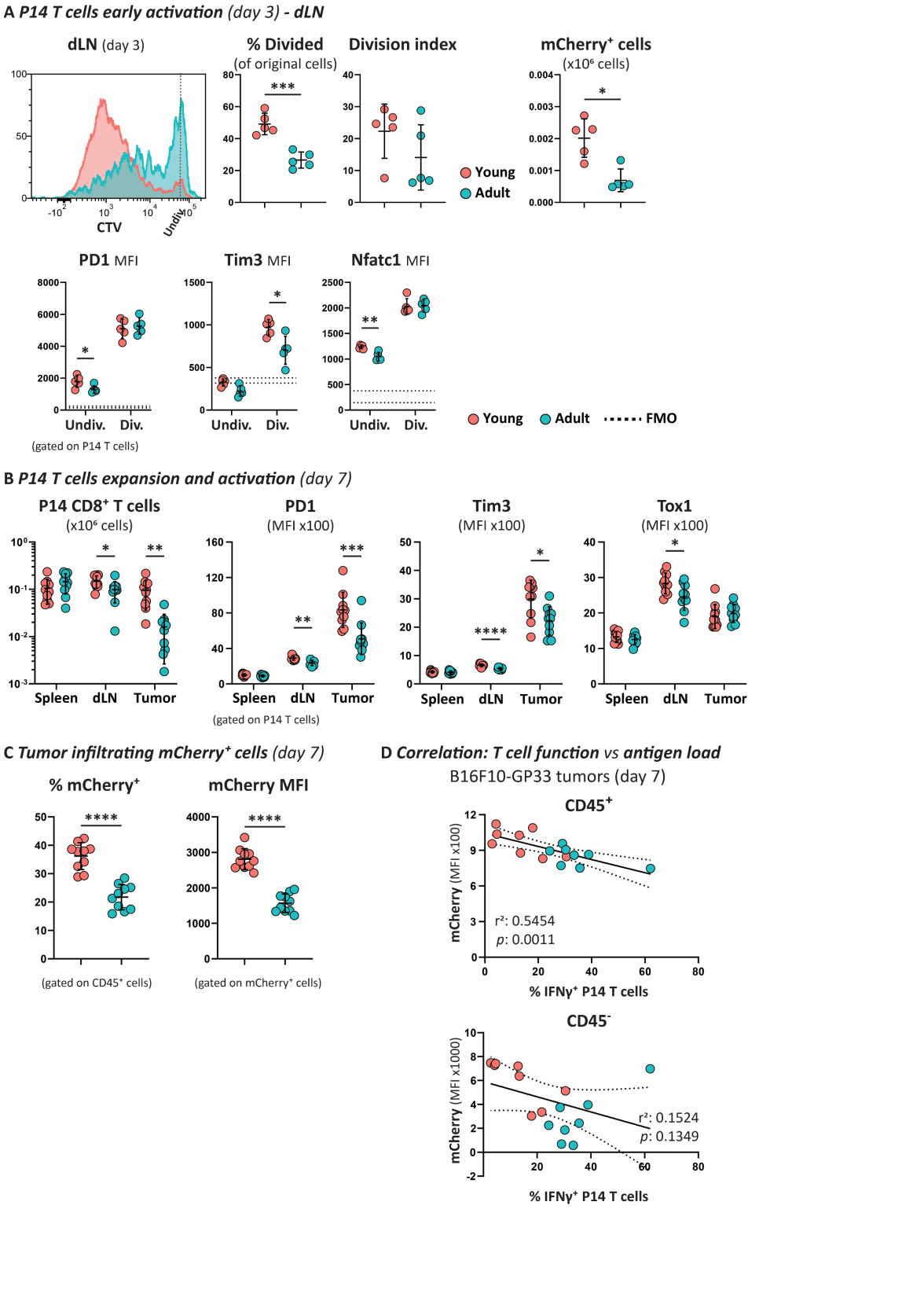
A P14 T cells early activation (day 3) - dLN
dLN (day 3)
CTV
Undiv.
% Divided
(of original cells)
Division index
mCherry+ cells
(x10⁶ cells)
Young
Adult
PD1 MFI
Tim3 MFI
Nfatc1 MFI
Undiv.
Div.
(gated on P14 T cells)
FMO
B P14 T cells expansion and activation (day 7)
P14 CD8+ T cells
(x10⁶ cells)
PD1
(MFI x100)
Tim3
(MFI x100)
Tox1
(MFI x100)
Spleen
dLN
Tumor
(gated on P14 T cells)
C Tumor infiltrating mCherry+ cells (day 7)
% mCherry+
mCherry MFI
(gated on CD45+ cells)
(gated on mCherry+ cells)
D Correlation: T cell function vs antigen load
B16F10-GP33 tumors (day 7)
CD45+
mCherry (MFI x100)
r²: 0.5454
p: 0.0011
% IFNγ+ P14 T cells
CD45-
mCherry (MFI x1000)
r²: 0.1524
p: 0.1349

Figure S3 Age related differences of CD8$^+$ T cell mediated immune response to B16F10-BKO-GP33 tumor model.

(**A**) CTV-labeled P14 CD8$^+$ T (100K) were adoptively transferred in young and adult mice (n=5 per group) one day before they were challenged with MHCI-deficient B16F10-GP33 cells. Proliferation and activation of P14 cells was assessed 3 days upon tumor challenge in the dLNs. The number of mCherry$^+$ cells in the dLNs was also calculated. Mean ±SD; unpaired parametric Welch t-test. The experiment was performed once.

(**B**) Naïve P14 CD8$^+$ T cells (20K) were adoptively transferred in young or adult mice (n=10 per group) one day before they were challenged with MHCI-deficient B16F10-GP33 tumor cells. Expansion and activation of P14 T cells was assessed 7 days post tumor challenge. Mean ±SD; multiple unpaired parametric Welch t-test. The experiment was performed once.

(**C**) Frequency and mCherry fluorescence intensity of myeloid cells infiltrating young or adult B16F10-BKO-GP33 tumors, 7 days post tumor challenge. Mean ±SD; unpaired parametric Welch t-test.

(**D**) Naïve P14 CD8$^+$ T cells (10K) were adoptively transferred in young or adult mice (n=8 per group) one day before they were challenged with MHCI-proficient B16F10-GP33 tumor cells. One week later the functionality of tumor infiltrating P14 T cells was assessed. The percent of IFNγ expressing P14 cells was inversely correlated with the mCherry intensity level of immune infiltrates but not that of the tumor cells. Simple linear regression analysis. The experiment was performed once.

A *p*-value of <0.05 is regarded as statistically significant, and different levels of significance are represented with asterisks: *P ≤ 0.05, **P ≤ 0.01, ***P ≤ 0.001, and ****P ≤ 0.0001.

Figure S4

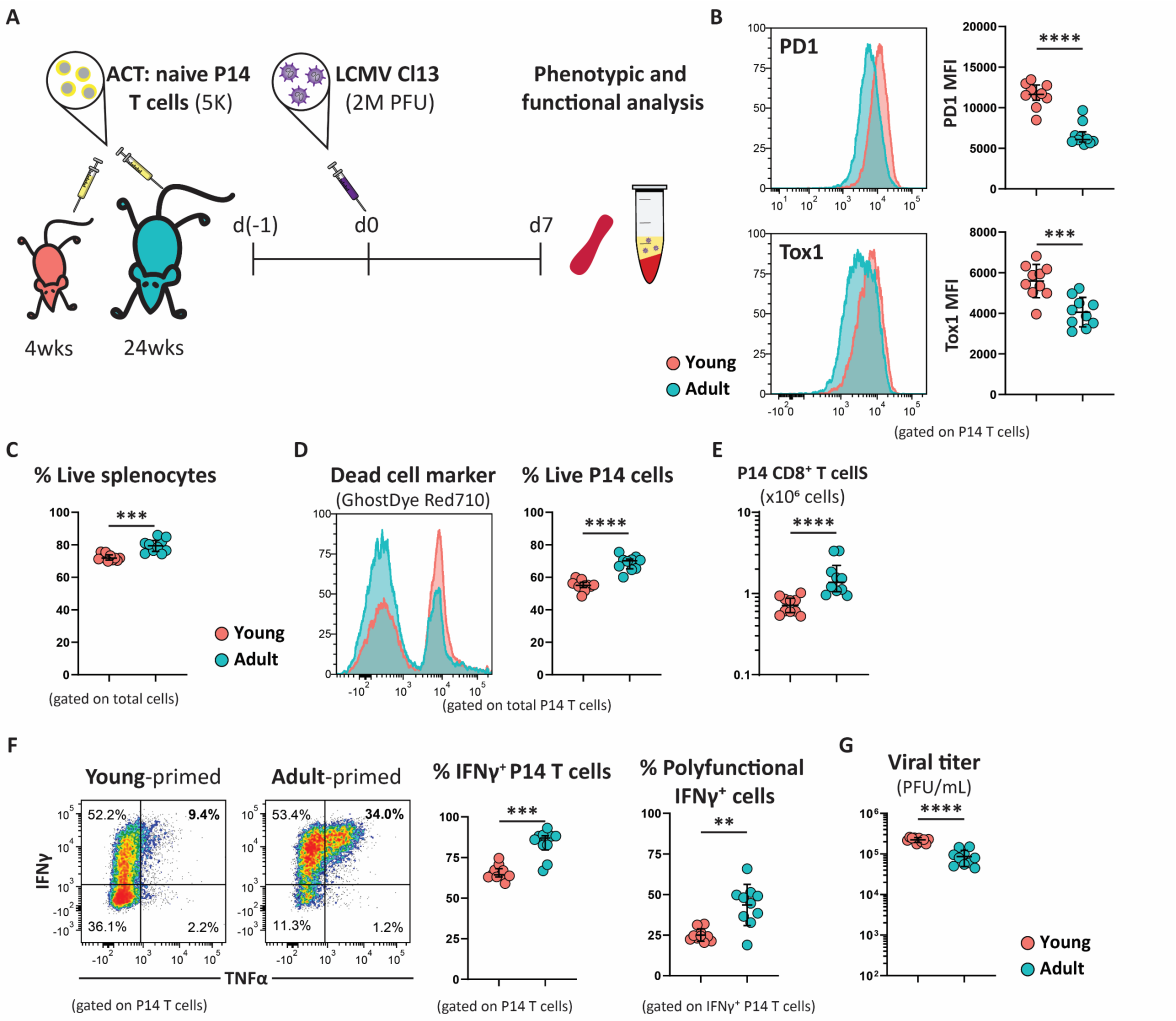
A
ACT: naive P14 T cells (5K)
LCMV Cl13 (2M PFU)
Phenotypic and functional analysis
d(-1)
d0
d7
4wks
24wks
B
PD1
Tox1
PD1 MFI
Tox1 MFI
Young
Adult
(gated on P14 T cells)
C
% Live splenocytes
(gated on total cells)
D
Dead cell marker
(GhostDye Red710)
% Live P14 cells
(gated on total P14 T cells)
E
P14 CD8⁺ T cells
(x10⁶ cells)
F
Young-primed
Adult-primed
IFNγ
TNFα
52.2%
9.4%
36.1%
2.2%
53.4%
34.0%
11.3%
1.2%
(gated on P14 T cells)
% IFNγ⁺ P14 T cells
(gated on P14 T cells)
% Polyfunctional IFNγ⁺ cells
(gated on IFNγ⁺ P14 T cells)
G
Viral titer
(PFU/mL)

Figure S4 $CD8^+$ T cell functional exhaustion is exacerbated in chronically infected young mice.

(**A**) Schematic experimental design: Five thousand naïve $CD90.1^+$ P14 $CD8^+$ T cells were adoptively transferred into young (4-weeks; n=10) or adult (24-weeks; n=10) C57Bl6 mice. One day later all mice were systematically challenged with 2M PFU of LCMV Cl13. Phenotypic and functional analysis was performed 7 days post infection. The experiment was performed once.

(**B**) Representative flow cytometry histogram plots (left) and summarized data (right) of the expression levels of PD1 and Tox1 by the transferred P14 $CD8^+$ T cells. Mean ±SD; unpaired Welch t-test.

(**C**) Frequency of live splenocytes from young and adult infected mice. Mean ±SD; unpaired Welch t-test.

(**D**) Representative flow cytometry histogram plots (left) and summarized data (right) of the frequency of live (dead cell marker negative) P14 $CD8^+$ T cells from the spleens of young and adult infected mice. Mean ±SD; unpaired Welch t-test.

(**E**) Total cell number of splenic P14 $CD8^+$ T cells expanded in the young or adult infected mice. Mean ±SD; unpaired Welch t-test.

(**F**) Representative flow cytometry density plots (left) and summarized data (right) of the cytokine response upon *ex vivo* stimulation of P14 $CD8^+$ T cells with GP33 peptide. Mean ±SD; unpaired Welch t-test.

(**G**) Viral titers of the peripheral blood plasma isolated from young or adult infected mice. Mean ±SD; unpaired Welch t-test.

A *p*-value of <0.05 is regarded as statistically significant, and different levels of significance are represented with asterisks: *$P \leq 0.05$, **$P \leq 0.01$, ***$P \leq 0.001$, and ****$P \leq 0.0001$.

Figure S5

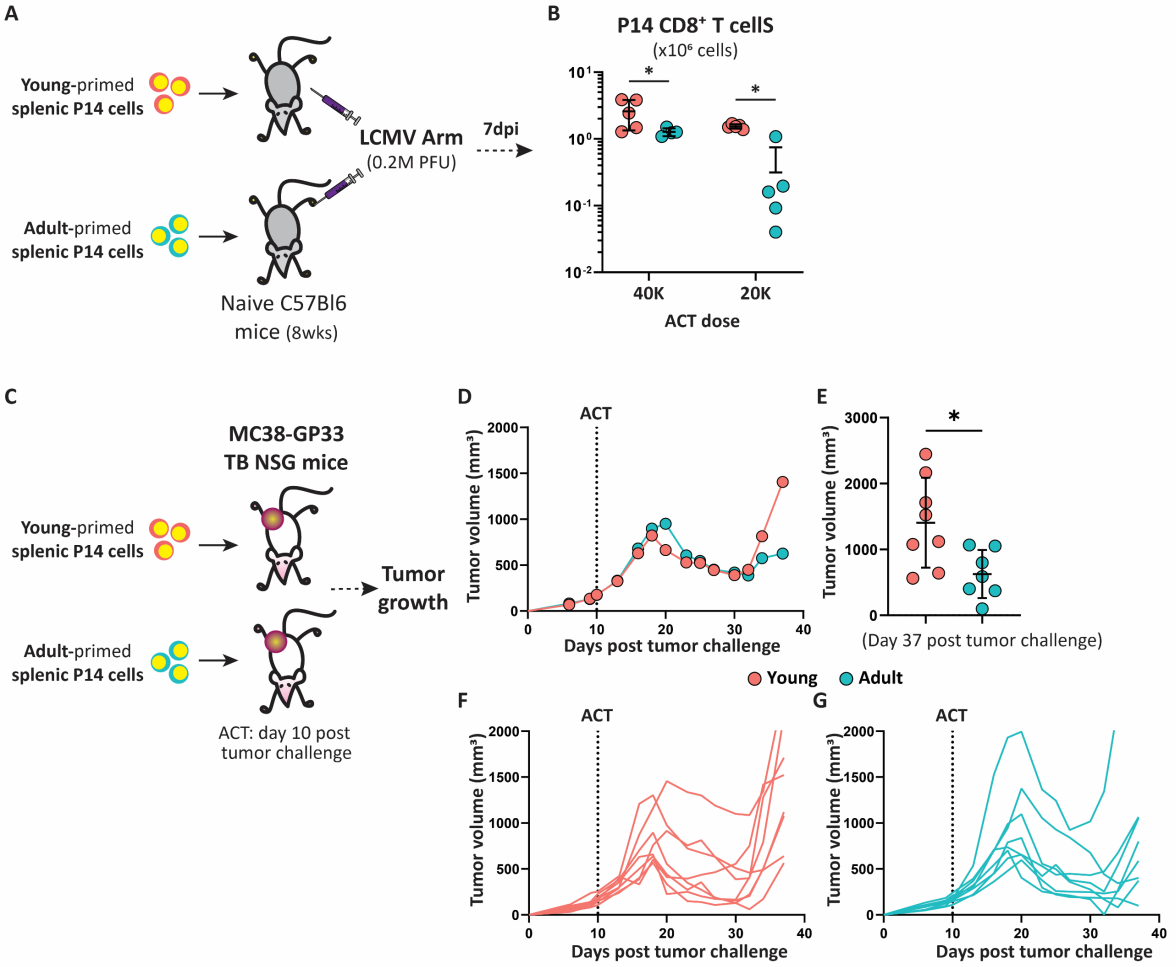
A
Young-primed splenic P14 cells
Adult-primed splenic P14 cells
LCMV Arm (0.2M PFU)
7dpi
Naive C57Bl6 mice (8wks)
B
P14 CD8+ T cellS (x10⁶ cells)
40K
20K
ACT dose
C
MC38-GP33 TB NSG mice
Young-primed splenic P14 cells
Adult-primed splenic P14 cells
Tumor growth
ACT: day 10 post tumor challenge
D
ACT
Tumor volume (mm³)
Days post tumor challenge
E
Tumor volume (mm³)
(Day 37 post tumor challenge)
Young
Adult
F
ACT
Tumor volume (mm³)
Days post tumor challenge
G
ACT
Tumor volume (mm³)
Days post tumor challenge

Figure S5 Young-primed CD8$^+$ T cells are skewed toward a terminal effector state.

(**A**) Schematic experimental design: young- or adult-primed P14 CD8$^+$ T cells, isolated from the spleens of TB mice at day 7, were adoptively transferred to naïve C57Bl6 mice at 2 different doses (40K and 20K). The next day the secondary hosts were challenged with LCMV Arm, and expansion of transferred cells was estimated 1 week later. The experiment was performed once.

(**B**) Total number of P14 CD8$^+$ T cells from the spleens of infected mice (n=5 per each group). Mean ±SD; multiple unpaired Welch t-test.

(**C**) Schematic experimental design: young- or adult-primed P14 CD8$^+$ T cells, isolated from the spleens of TB mice at day 7, were transferred to MC38-GP33 TB immunocompromised mice (day 10 post tumor challenge).

(**D**) Mean tumor growth kinetics of NSG mice.

(**E**) Tumor volumes of NSG mice at day 37. Mean ±SD; unpaired Welch t-test.

(**F**) Tumor growth kinetics of individual mice per each age group (n=8).

A *p*-value of <0.05 is regarded as statistically significant, and different levels of significance are represented with asterisks: *P ≤ 0.05, **P ≤ 0.01, ***P ≤ 0.001, and ****P ≤ 0.0001.

Figure S6

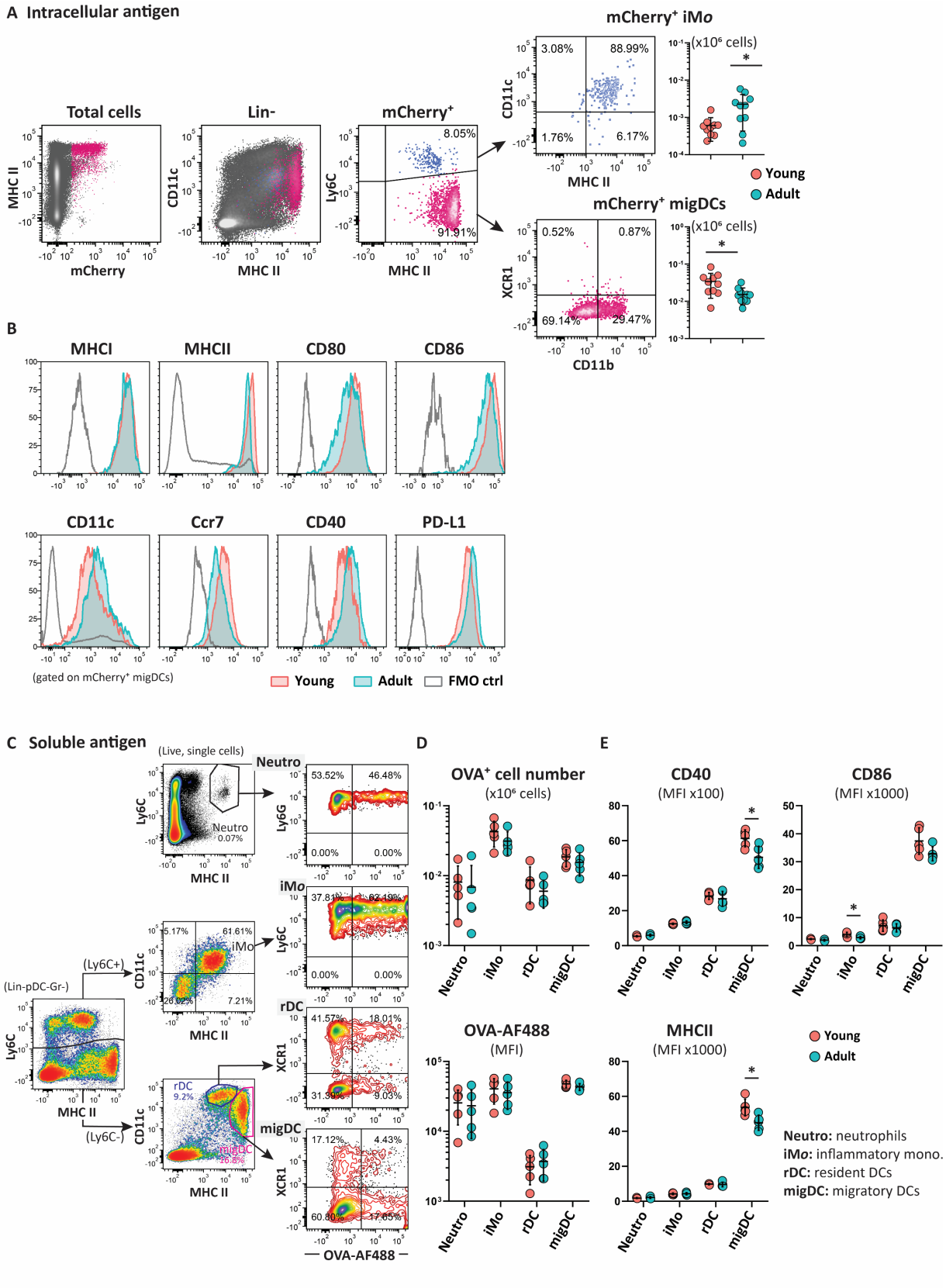
A Intracellular antigen
Total cells
Lin-
mCherry+
mCherry+ iMo
mCherry+ migDCs
(x10⁶ cells)
Young
Adult
B
MHCI
MHCII
CD80
CD86
CD11c
Ccr7
CD40
PD-L1
(gated on mCherry+ migDCs)
Young
Adult
FMO ctrl
C Soluble antigen
(Live, single cells)
Neutro
iMo
rDC
migDC
(Ly6C+)
(Ly6C-)
(Lin-pDC-Gr-)
OVA-AF488
D
OVA+ cell number
(x10⁶ cells)
OVA-AF488
(MFI)
E
CD40
(MFI x100)
CD86
(MFI x1000)
MHCII
(MFI x1000)
Neutro
iMo
rDC
migDC
Young
Adult
Neutro: neutrophils
iMo: inflammatory mono.
rDC: resident DCs
migDC: migratory DCs

Figure S6 Composition and abundance of APCs that uptake and transfer antigen to the dLN of young and adult mice.

(**A**) Young (4-weeks old; n=10) and adult (24-weeks old; n=10) C57Bl6 mice were inoculated s.c. with apoptotic MC38-GP33-BKO cells, and the APCs present in the draining lymph nodes were analyzed 18 hours later. Representative flow cytometry plots showing the phenotype of $mCherry^+$ DCs from the dLNs of young and adult mice. Mean ±SD; unpaired Welch t-test.

(**B**) Representative histogram plots showing the expression of the indicated markers on the cell surface of the $mCherry^+$ migDCs from the dLNs of young and adult mice from (A). The gray line shows the autofluorescence level of the corresponding channel of the appropriate FMO control sample; for the MHCII and CD11c markers, which are used to define the migDC subset, the gray line shows the expression of MHCII and CD11c on total $CD11b^+$ cells.

(**C**) Young (4-weeks old; n=5) and adult (24-weeks old; n=5) C57Bl6 mice were vaccinated s.c. with OVA-AF488 protein emulsified in CFA, and APCs present in the draining lymph nodes were analyzed 18 hours later. Representative flow cytometry plots showing the gating strategy of myeloid subsets that have captured OVA protein. [neutro: neutrophils; iMo: inflammatory monocytes; rDC: resident DC; migDC: migratory DC]

(**D**) Total cell number (left) and fluorescent intensity (right) of the OVA^+ fraction of the indicated cell subsets isolated from the dLN of young or adult mice. Mean ±SD; multiple unpaired Welch t-test.

(**E**) Summarized data showing the expression intensity of activation markers on the indicated cell subsets. Mean ±SD; multiple unpaired Welch t-test.

A *p*-value of <0.05 is regarded as statistically significant, and different levels of significance are represented with asterisks: *P ≤ 0.05, **P ≤ 0.01, ***P ≤ 0.001, and ****P ≤ 0.0001.

Figure S7

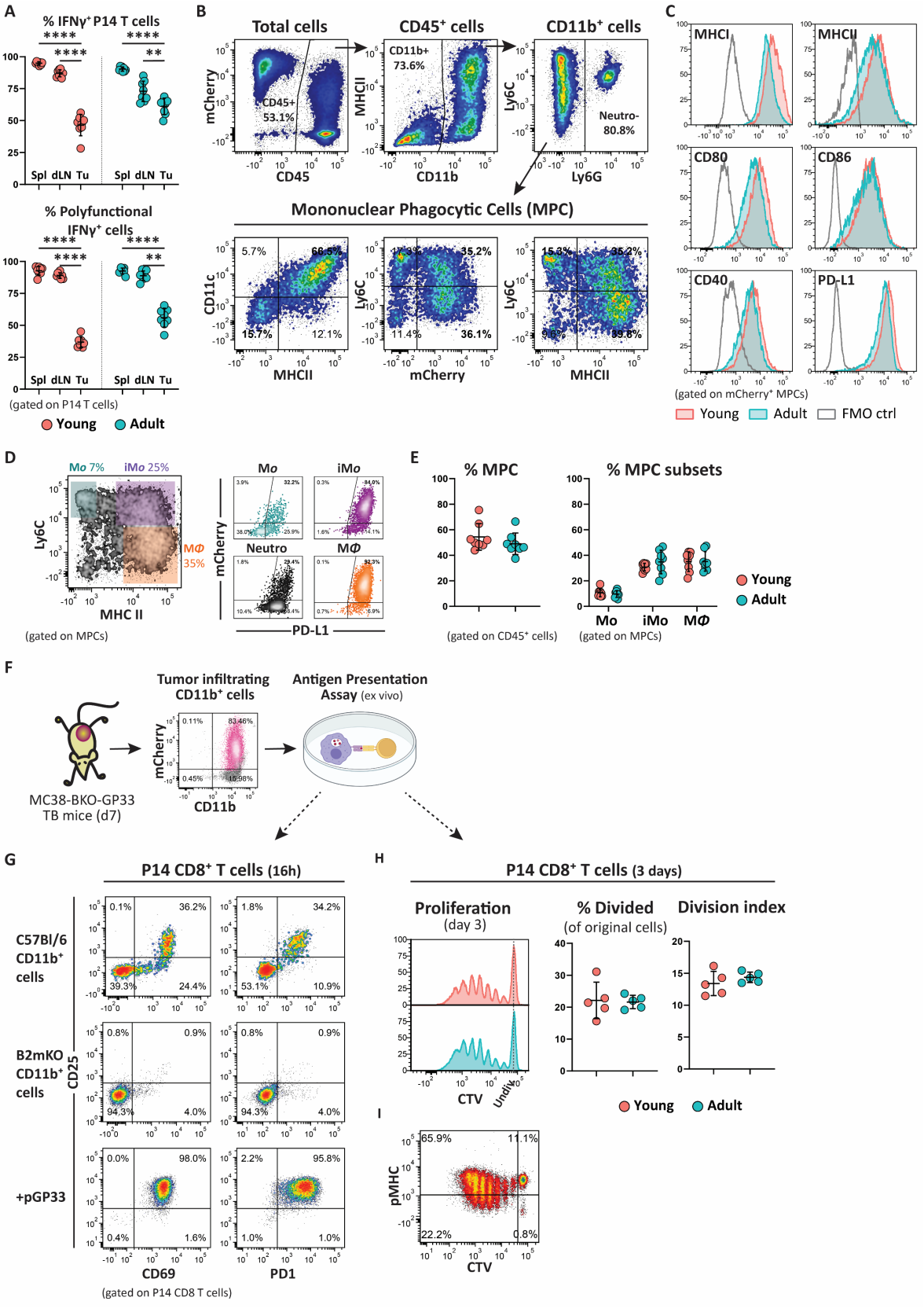
A
% IFNγ+ P14 T cells
Spl dLN Tu Spl dLN Tu
% Polyfunctional IFNγ+ cells
(gated on P14 T cells)
Young
Adult
B
Total cells
CD45+ cells
CD11b+ cells
CD45+ 53.1%
CD11b+ 73.6%
Neutro- 80.8%
Mononuclear Phagocytic Cells (MPC)
C
MHCI
MHCII
CD80
CD86
CD40
PD-L1
(gated on mCherry+ MPCs)
Young
Adult
FMO ctrl
D
Mo 7%
iMo 25%
MΦ 35%
MHC II
(gated on MPCs)
Mo
iMo
Neutro
MΦ
PD-L1
E
% MPC
% MPC subsets
(gated on CD45+ cells)
(gated on MPCs)
Young
Adult
F
Tumor infiltrating CD11b+ cells
Antigen Presentation Assay (ex vivo)
MC38-BKO-GP33 TB mice (d7)
G
P14 CD8+ T cells (16h)
C57Bl/6 CD11b+ cells
B2mKO CD11b+ cells
+pGP33
CD25
CD69
PD1
(gated on P14 CD8 T cells)
H
P14 CD8+ T cells (3 days)
Proliferation (day 3)
% Divided (of original cells)
Division index
CTV
Young
Adult
I
pMHC
CTV

Figure S7 Young tumor-infiltrating MPCs are more efficient at cross-presenting tumor antigens.

(**A**) Summarized data showing cytokine production by young- and adult-primed P14 TILs from peripheral lymphoid tissues and tumors, upon 4h ex vivo stimulation with GP33 peptide. Mean ±SD; multiple unpaired Welch t-test.

(**B**) Representative flow cytometry density plots showing the gating strategy for identification and characterization of mononuclear phagocytic cells (MPCs) from MC38-GP33-BKO tumors established for 7 days in C57Bl/6 mice.

(**C**) Representative histogram plots showing the expression of the indicated markers on the surface of mCherry^{+} MPCs from young or adult tumors. The gray lines represent the autofluorescence for the corresponding channel based on FMO control samples.

(**D**) Representative flow cytometry density plots showing immunophenotypic characterization of MPC subsets (left) and their ability to uptake tumor antigen (mCherry fluorescence) and express PD-L1 (right). (M*o*: monocytes; iM*o*: inflammatory monocytes; M*Φ*: macrophages)

(**E**) Summarized data showing the frequency of MPCs and their cellular composition in young and adult TB hosts. Mean ±SD; multiple unpaired Welch t-test.

(**F**) Schematic experimental design of the antigen cross-presentation assay as in Fig. 4C.

(**G**) Representative flow cytometry density plots showing the activation of P14 CD8^{+} T cells one day upon ex vivo stimulation with tumor infiltrating CD11b^{+} cells from experimental mice (top row) or control B2mKO mice (middle row). Bottom row shows the activation of P14 cells upon addition of synthetic pGP33 peptide.

(**H**) Proliferation of CTV-labeled P14 CD8^{+} T cells 3 days upon ex vivo stimulation with CD11b^{+} tumor infiltrating myeloid cells. Mean ±SD; unpaired Welch t-test.

(**I**) Representative density plot showing the density of TCR complex on the surface of P14 CD8^{+} T cells as a function of cell divisions.

A *p*-value of <0.05 is regarded as statistically significant, and different levels of significance are represented with asterisks: *P ≤ 0.05, **P ≤ 0.01, ***P ≤ 0.001, and ****P ≤ 0.0001.

Figure S8

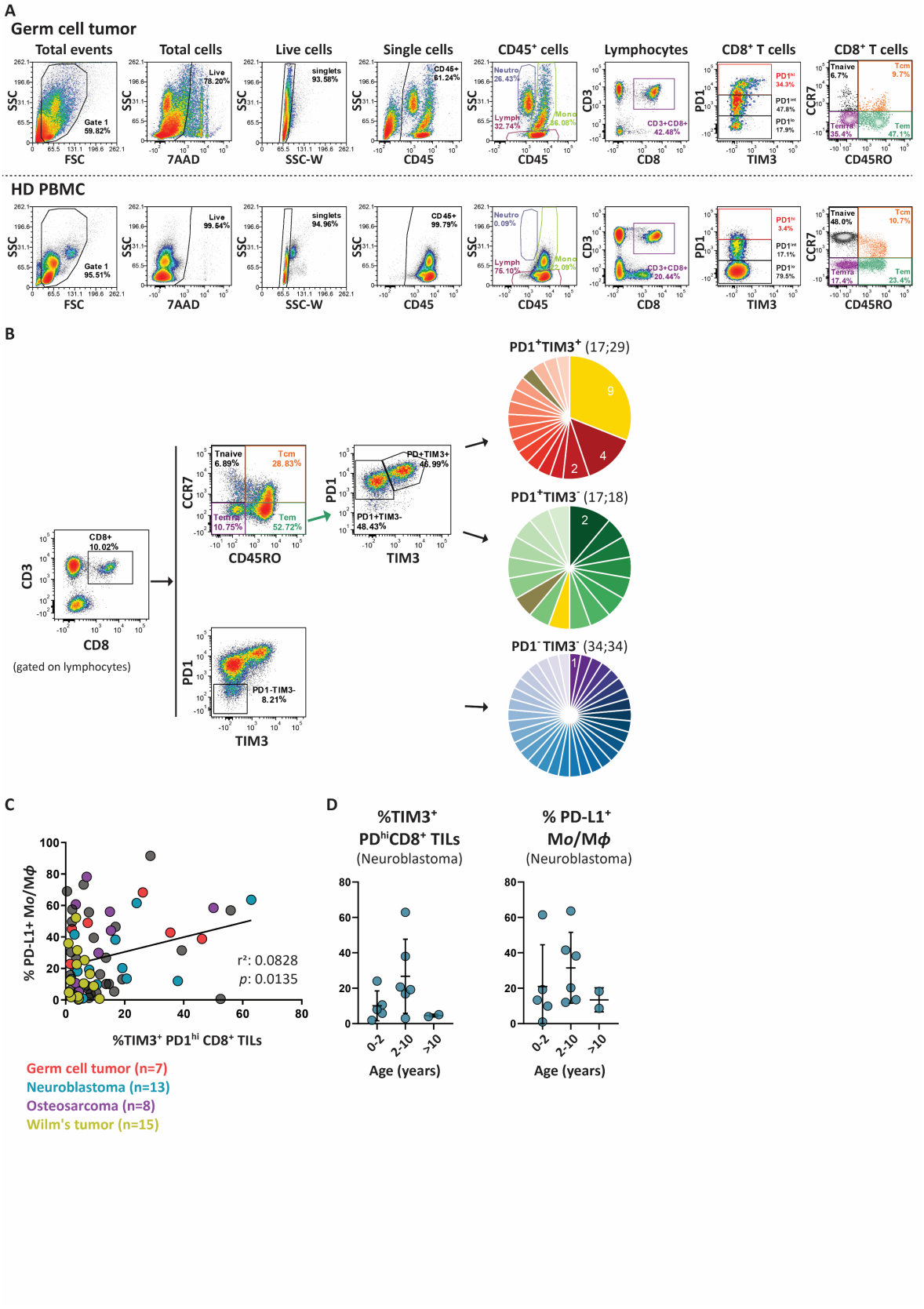
A
Germ cell tumor
Total events
Total cells
Live cells
Single cells
CD45+ cells
Lymphocytes
CD8+ T cells
CD8+ T cells
Gate 1 59.82%
Live 78.20%
singlets 93.58%
CD45+ 61.24%
Neutro 26.43%
Lymph 32.74%
Mono 36.08%
CD3+CD8+ 42.48%
PD1hi 34.3%
PD1int 47.8%
PD1lo 17.9%
Tnaive 6.7%
Tcm 9.7%
Temra 35.4%
Tem 47.1%
FSC
SSC
7AAD
SSC-W
CD45
CD8
TIM3
CD45RO
CCR7
PD1
CD3
HD PBMC
Gate 1 95.51%
Live 99.64%
singlets 94.96%
CD45+ 99.79%
Neutro 0.09%
Lymph 75.10%
Mono 2.09%
CD3+CD8+ 20.44%
PD1hi 3.4%
PD1int 17.1%
PD1lo 79.5%
Tnaive 48.0%
Tcm 10.7%
Temra 17.4%
Tem 23.4%
B
CD8+ 10.02%
(gated on lymphocytes)
Tnaive 6.89%
Tcm 28.83%
Temra 10.75%
Tem 52.72%
PD1+TIM3+ 46.99%
PD1+TIM3- 48.43%
PD1-TIM3- 8.21%
PD1+TIM3+ (17;29)
PD1+TIM3- (17;18)
PD1-TIM3- (34;34)
C
% PD-L1+ Mo/Mϕ
%TIM3+ PD1hi CD8+ TILs
r²: 0.0828
p: 0.0135
Germ cell tumor (n=7)
Neuroblastoma (n=13)
Osteosarcoma (n=8)
Wilm's tumor (n=15)
D
%TIM3+ PDhiCD8+ TILs
(Neuroblastoma)
% PD-L1+ Mo/Mϕ
(Neuroblastoma)
0-2
2-10
>10
Age (years)

Figure S8 $CD8^+$ T cells infiltrating pediatric solid tumors are enriched in antigen-experienced cells.

(**A**) Flow cytometry "nested" gating strategy to identify and profile tumor infiltrating $CD8^+$ T cells (top row). Equivalent gating strategy performed on PBMCs from a healthy donor (HD) is shown for reference (bottom row). The current gate for the displayed events in each plot is indicated on top.

(**B**) Analysis of TCR repertoire diversity and clonotype composition of among $CD8^+$ TILs (Germ cell tumor sample) with different expression levels of inhibitory receptors, PD1 and TIM3 (see sorting strategy on the left). Each a/b clonotype is represented by a single pie-slice proportional to its frequency. Common clonotypes among different $CD8^+$ phenotypes are represented by the same color.

(**C**) Correlation between the frequency of TIM3 expressing $PD1^{high}$ $CD8^+$ TILs and the percentage of monocyte/macrophages that express PDL1 (n=73). Distribution of the most represented tumor types is indicated (color coded). Simple linear regression analysis.

(**D**) Frequency of TIM3 expressing $PD1^{high}$ $CD8^+$ TILs (left) and the percentage of monocyte/macrophages that express PDL1 (right) from 13 neuroblastoma tumor samples among different age groups. Mean ±SD; unpaired Kruskal-Wallis test with Dunn's correction.

A *p*-value of <0.05 is regarded as statistically significant, and different levels of significance are represented with asterisks: *P ≤ 0.05, **P ≤ 0.01, ***P ≤ 0.001, and ****P ≤ 0.0001.

Supplementary table

Antibodies used in this study:

Antibody	Clone	Source	Catalog #	Antibody ID
anti-mouse KLRG1-AF488	2F1	BD	561619	AB_10898017
anti-mouse CD274-BV421	MIH5	BD	564716	AB_2738911
anti-mouse TNF-BV421	MP6-XT22	BD	563387	AB_2738173
anti-mouse CD44-BV510	IM7	BD	563114	AB_2738011
anti-mouse CD45-BV786	30-F11	BD	564225	AB_2716861
anti-mouse IFNγ-APC	XMG1.2	BD	554413	AB_398551
anti-human/mouse Ki67-BV786	B56	BD	563756	AB_2732007
anti-mouse IL-2-AF488	JES6-5H4	BD	557725	AB_396833
anti-mouse CD11b-BV510	M1/70	BD	562950	AB_2737913
anti-mouse CD127-BV421	A7R34	BD	566377	AB_2739717
anti-mouse CD90.1-PerCP	OX-7	BD	557266	AB_396611
7AAD	n/a	BD	559925	n/a
anti-human PDL1-BV786	MIH1	BD	563739	AB_2738397
anti-mouse PD1-PE	29F.1A12	BioLegend	135206	AB_1877231
anti-mouse CD8a-APC-Fire750	53-6.7	BioLegend	100766	AB_2572113
anti-human/mouse Granzyme B-PacBlue	GB11	BioLegend	515408	AB_2562196
anti-mouse CD62L-BV605	MEL-14	BioLegend	104438	AB_2563058
anti-mouse IA/IE-FITC	M5/114.15.2	Biolegend	107606	AB_313321
anti-human/mouse CD45R/B220-PerCP	RA3-6B2	Biolegend	103234	AB_893353
anti-mouse F4/80-PE	BM8	Biolegend	123110	AB_893486
anti-mouse CD11c-PECy7	N418	Biolegend	117318	AB_493568
anti-mouse Ly-6C-APC-Fire750	HK1.4	Biolegend	128046	AB_2616731
anti-mouse Ly-6G-BV605	1A8	Biolegend	127639	AB_2565880
anti-human CD39-BV510	A1	Biolegend	328219	AB_2563265
anti-human CCR7-AF488	G043H7	Biolegend	353206	AB_10916389
anti-human PD1-PE	EH12.2H7	Biolegend	329906	AB_940483
anti-human TIM3-PE	F38-2E2	Biolegend	345014	AB_2561720
anti-human CD45RO-APC	UCHL1	Biolegend	304210	AB_314426
anti-human CD3-APC-Cy7	SK7	Biolegend	344818	AB_10645474
anti-human CD8α-BV421	RPA-T8	Biolegend	301036	AB_10960142
anti-human CD45-BV605	HI30	Biolegend	304042	AB_2562106
anti-mouse H2-D/Kb-AF647	28-8-6	Biolegend	114612	AB_492931
anti-mouse CD25-PE	3C7	BioLegend	101904	AB_312847
anti-mouse CD69-BV605	H1.2F3	BioLegend	104530	AB_11203710
anti-mouse Ccr7-AF488	4B12	BioLegend	120110	AB_492841
anti-mouse Xcr1-BV421	ZET	BioLegend	148216	AB_2565230
anti-mouse CD64-PE	X54-5/7.1	Biolegend	139304	AB_10612740

Antibody	Clone	Source	Catalog #	Antibody ID
anti-mouse CD80-PE	16-10A1	Biolegend	104708	AB_313129
anti-mouse CD40-AF488	HM40-3	Biolegend	102910	AB_492852
anti-mouse CD86-BV421	GL-1	Biolegend	105032	AB_2650895
anti-human/mouse Nfatc1-AF488	7A6	Biolegend	649604	AB_2561823
anti-human/mouse Irf4-AF647	IRF4.3E4	Biolegend	646408	AB_2564047
Annexin V-PE-Cy7		Biolegend	640950	
anti-mouse CD206-PerCP-Cy5.5	C068C2	Biolegend	141716	AB_2561992
anti-mouse/human TCF7-AF488	C63D9	Cell Signaling	6444S	AB_2797627
anti-human/mouse Tcf7-AF488	C63D9	Cell Signaling	6444S	AB_2797627
anti-mouse Tim3-PeCy7	RMT3-23	eBioscience	25-5870-82	AB_2573483
anti-human/mouse TOX1-eFluor660	TXRX10	eBioscience	50-6502-82	AB_2574265
anti-mouse CD39-PerCP-eFluor710	24DMS1	eBioscience	46-0391-82	AB_10717953
anti-mouse Nur77-AF488	12.14	eBioscience	53-5965-82	AB_2574429
anti-human/mouse Arginase1-AF488	A1exF5	eBioscience	53-3697-82	AB_2734831
anti-human/mouse Tox-APC	TXRX10	eBioscience	50-6502-82	AB_2574265
anti-mouse iNOS-APC	REA982	Miltenyi	130-116-359	AB_2727487
anti-human/mouse Tox-APC	REA473	Miltenyi	130-118-335	AB_2751485
Ghost Dye Red 710	n/a	Tonbo	13-0871-T500	n/a
anti-mouse TCRbeta-PerCP-Cy5.5	H57-597	Tonbo	65-5961-U100	AB_2621911
anti-mouse NK1.1-PerCPCy5.5	PK136	Tonbo	65-5941-U100	AB_2621910
anti-human/mouse B220-PerCP-Cy5.5	RA3-6B2	Tonbo	65-0452-U100	AB_2621892
anti-mouse CD19-PerCP-Cy5.5	1D3	Tonbo	65-0193-U100	AB_2621887

213